

Assessing the Calibration of High-Dimensional Ensemble Forecasts Using Rank Histograms

Thordis L. Thorarinsdottir*, Michael Scheuerer[†] and Christopher Heinz[‡]

Abstract

Any decision making process that relies on a probabilistic forecast of future events necessarily requires a calibrated forecast. This paper proposes new methods for empirically assessing forecast calibration in a multivariate setting where the probabilistic forecast is given by an ensemble of equally probable forecast scenarios. Multivariate properties are mapped to a single dimension through a pre-rank function and the calibration is subsequently assessed visually through a histogram of the ranks of the observation's pre-ranks. Average ranking assigns a pre-rank based on the average univariate rank while band depth ranking employs the concept of functional band depth where the centrality of the observation within the forecast ensemble is assessed. Several simulation examples and a case study of temperature forecast trajectories at Berlin Tegel Airport in Germany demonstrate that both multivariate ranking methods can successfully detect various sources of miscalibration and scale efficiently to high dimensional settings.

Keywords: average rank; band depth; forecast trajectory; forecast verification; modified band depth; multivariate forecast

1 Introduction

Calibration, the statistical compatibility between a probabilistic forecast and the realized observation, is a fundamental property of any skillful forecast. Formally, we say that the forecast is calibrated if, over the long run, events assigned a given probability are realized with the same empirical frequency. Calibration is thus a critical requirement for optimal decision making and any decision aiding technique that relies on the forecast (Lichtenstein et al., 1977; Gneiting et al., 2007).

In the case of a univariate probabilistic forecast given by a continuous predictive distribution, Dawid (1984) proposes the use of the probability integral transform (PIT) for calibration assessment. That is, if the distribution F is a calibrated forecast for the observation y , it holds that $F(y) \sim \mathcal{U}([0, 1])$. A randomized version of the PIT that applies to partly, or fully, discrete distributions is discussed in Czado et al. (2009). For an ensemble of deterministic forecasts that

*Norwegian Computing Center. *Corresponding author:* thordis@nr.no

[†]Heidelberg University

[‡]Ulm University

approximate the predictive distribution, an equivalent tool is the rank of the observation y in the forecast ensemble x_1, \dots, x_{m-1} (Anderson, 1996; Hamill and Colucci, 1997). The calibration of a large number of forecast cases may then be assessed empirically by plotting the histogram of the resulting PIT values or verification ranks (Gneiting et al., 2007). If the forecasts lack calibration, the shape of the PIT or the verification rank histogram may reveal the nature of the misspecification and thus provide a useful guidance to the improvement of the forecasting method. For instance, a \cup -shaped histogram is an indication of underdispersion while a \cap -shape suggests overdispersion.

To assess the calibration of multivariate ensemble forecasts, Gneiting et al. (2008) propose a multivariate ranking method that proceeds in two steps. In the first step, the observation and the ensemble members are assigned pre-ranks based on a rank structure equal to that of the empirical copula. The multivariate rank of the observation is then given by the rank of its pre-rank. A recent extension that applies to full distributions is given in Ziegel and Gneiting (2013). While the multivariate rank histogram has been shown to work well for low-dimensional forecasts, see e.g. Schuhen et al. (2012) and Möller et al. (2013), the multivariate ordering in the first step seems to lack power in higher dimensions (Pinson and Girard, 2012). Alternative methods for high-dimensional calibration assessment are thus in demand (Pinson, 2013; Schefzik et al., 2013).

To this end, we propose two pre-ranking methods that complement the technique of Gneiting et al. (2008). These methods are based on the concept of band depth for functional data introduced by López-Pintado and Romo (2009) which relates to the graphical representation of the functional data curves. That is, continuous or discrete curves are given a center-outward ordering according to the centrality of a curve within the collection of sample curves. Sun and Genton (2011, 2012) apply this concept to develop a box plot for the visualization and outlier-detection of functional data. Viewing a discrete curve of length d as a point in d -dimensional space, we define a pre-ranking method based on the band depth concept of López-Pintado and Romo (2009). In the discrete case, the band depth essentially corresponds to the average centrality of the d points. As a second alternative, we thus also consider a pre-rank given by the average of the univariate ranks.

The remainder of the paper is organized as follows. In Section 2, we review the concept of band depth for discrete data and define the two multivariate ranking methods. Section 3 and 4 provide the results of simulation studies where we investigate the influence of dimensionality and correlation, respectively, on the band depth ranks, the average ranks and the technique of Gneiting et al. (2008). A further comparison of these three techniques is provided in Section 4, where we assess the calibration of temporal trajectories of temperature forecasts over Germany. The paper then ends with a discussion in Section 5.

2 Ranking multivariate data

Let $S = \{\mathbf{x}_1, \dots, \mathbf{x}_m\}$ denote a set of points in \mathbb{R}^d or a d -dimensional subset thereof, with $\mathbf{x}_i = (x_{i1}, \dots, x_{id})$. Here, we can think of S as comprising an ensemble forecast with $m - 1$ ensemble members and the corresponding observation $\mathbf{y} = \mathbf{x}_m$. Following the general set-up of Gneiting et al. (2008), the rank of the observation in S is calculated in two steps,

- (i) apply a pre-rank function $\rho_S : \mathbb{R}^d \rightarrow \mathbb{R}_+$ to calculate the pre-rank, $\rho_S(\mathbf{x})$, of every $\mathbf{x} \in S$;
- (ii) set the rank of \mathbf{x}_m equal to the rank of $\rho_S(\mathbf{x}_m)$ in $\{\rho_S(\mathbf{x}_1), \dots, \rho_S(\mathbf{x}_m)\}$ with ties resolved at random.

In Gneiting et al. (2008), the pre-rank function ρ_S is given by

$$\rho_S(\mathbf{x}) = \sum_{i=1}^m \mathbb{1}\{\mathbf{x}_i \preceq \mathbf{x}\}, \quad (1)$$

where $\mathbb{1}$ denotes the indicator function and $\mathbf{x}_i \preceq \mathbf{x}$ if and only if $x_{ik} \leq x_k$ for all $k = 1, \dots, d$. The authors further consider an optional initial step in the ranking procedure in which the data is normalized in each component before the ranking. As the pre-rank functions proposed below are invariant to such pre-processing, we omit this step here.

2.1 Band depth rank

López-Pintado and Romo (2009) introduce a center-outward ordering of curves which they call band depth. In the discrete case, it is defined as the proportion of coordinates of $\mathbf{x} \in S$ inside bands defined by subsets of n points from S ,

$$\begin{aligned} \text{bd}_S^n(\mathbf{x}) &= \binom{m}{n}^{-1} \frac{1}{d} \sum_{k=1}^d \sum_{1 \leq i_1 < \dots < i_n \leq m} \mathbb{1}\{\min\{x_{i_1 k}, \dots, x_{i_n k}\} \leq x_k\} \\ &\quad \times \mathbb{1}\{x_k \leq \max\{x_{i_1 k}, \dots, x_{i_n k}\}\}. \end{aligned} \quad (2)$$

Note that López-Pintado and Romo (2009) refer to this version of the definition as modified band depth, in reference to the corresponding definition for continuous curves. It holds that $0 \leq \text{bd}_S^n(\mathbf{x}) \leq 1$ for all $\mathbf{x} \in S$ and it gets closer to 1 the deeper, or more central, the point \mathbf{x} is in the set S . The depth is very stable in n and we thus only consider the case $n = 2$ which is equal to the simplicial depth of Liu (1990) and computationally very efficient (López-Pintado and Romo, 2009; Sun et al., 2013).

From (2), we obtain the band depth pre-rank function

$$\begin{aligned} \rho_S^{\text{bd}}(\mathbf{x}) &= \frac{1}{d} \sum_{k=1}^d \sum_{1 \leq i_1 < i_2 \leq m} \mathbb{1}\{\min\{x_{i_1 k}, x_{i_2 k}\} \leq x_k \leq \max\{x_{i_1 k}, x_{i_2 k}\}\} \\ &= \frac{1}{d} \sum_{k=1}^d \left[\text{rank}_S(x_k) [m - \text{rank}_S(x_k)] + [\text{rank}_S(x_k) - 1] \sum_{i=1}^m \mathbb{1}\{x_{ik} = x_k\} \right], \end{aligned} \quad (3)$$

where $\text{rank}_S(x_k) = \sum_{i=1}^m \mathbb{1}\{x_{ik} \leq x_k\}$ denotes the rank of the k th coordinate of \mathbf{x} in S . If $x_{ik} \neq x_{jk}$ with probability 1 for all $i, j \in \{1, \dots, m\}$ with $i \neq j$ and $k = 1, \dots, d$, the band depth pre-rank function in (3) further simplifies to

$$\rho_S^{\text{bd}}(\mathbf{x}) = \frac{1}{d} \sum_{k=1}^d [m - \text{rank}_S(x_k)] [\text{rank}_S(x_k) - 1] + (m - 1), \quad (4)$$

see also Sun et al. (2013).

It is straightforward to see that the band depth rank of an observation $\mathbf{y} = \mathbf{x}_m$ is uniformly distributed if $\mathbf{x}_1, \dots, \mathbf{x}_m$ are independent and identically distributed, which implies a calibrated

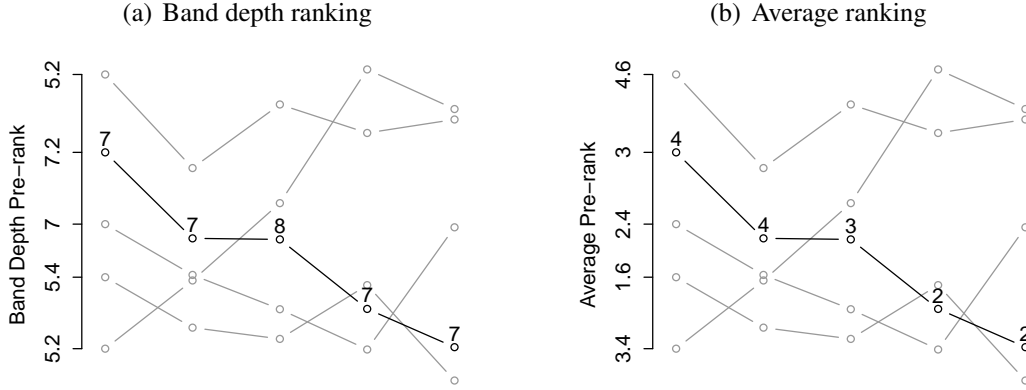


Figure 1: Illustration of (a) band depth, and (b) average pre-ranking for a multivariate temporal trajectory with $d = 5$ time points. The resulting pre-ranks are given on the y -axes. The four ensemble forecast curves are indicated in gray and the observation curve in black. The numbers next to each point of the observation curve indicate the univariate pre-ranks.

ensemble forecast. However, the interpretation of the resulting rank histogram is somewhat different than that of the classical univariate verification rank histogram. As the example in Figure 1(a) shows, the band depth pre-rank assesses the centrality of the elements in S , with the most central element(s) attaining the highest rank(s) and the most outlying element(s) attaining the lowest rank(s). A skew histogram with too many high ranks is thus an indication of an overdispersive ensemble while too many low ranks can result from either an underdispersive or biased ensemble. As demonstrated in the simulation study in Section 4, a lack of correlation in the ensemble will result in a \cap -shaped histogram while an ensemble with too high correlations produces a \cup -shaped histogram.

2.2 Average rank

The average rank is simply given by the average over the univariate ranks,

$$\rho_S^a(\mathbf{x}) = \frac{1}{d} \sum_{k=1}^d \text{rank}_S(x_k). \quad (5)$$

An illustration of the average pre-ranking is given in Figure 1. It follows directly from (5) that the resulting rank of \mathbf{x}_m in S is uniform on $\{1, \dots, m\}$ if the elements of S are independent and identically distributed. The average rank furthermore reduces to the classical univariate rank when $d = 1$.

The interpretation of the resulting histogram is similar to that of the univariate verification rank histogram. That is, if the forecasts are underdispersive the average rank histogram for the observation is \cup -shaped, an overdispersive ensemble results in a \cap -shaped histogram while a constant bias results in a triangular shaped histogram. As discussed in Section 4 under- and overestimation of the correlation structure can furthermore result in over- and underdispersive histograms, respectively.

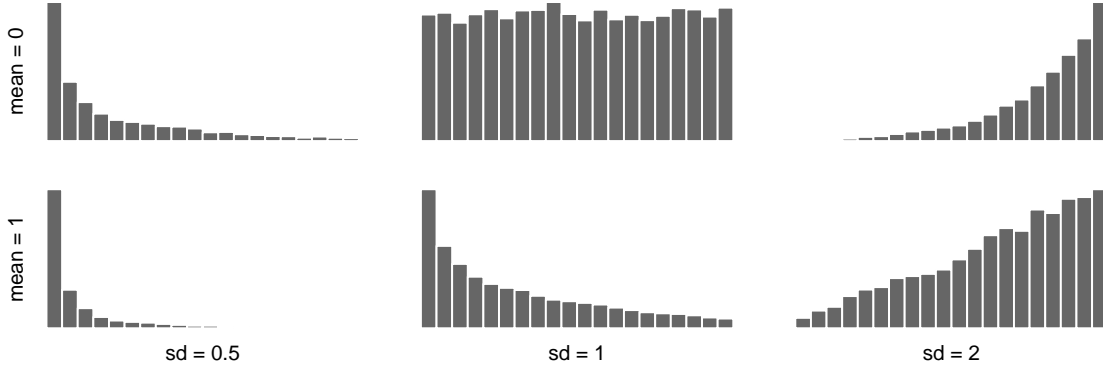


Figure 2: Band depth rank histograms for observations in $d = 3$ dimensions that follow independent standard Gaussian distributions while the 19 ensemble members follow independent Gaussian distributions with parameters as indicated. The results are based on 10000 repetitions.

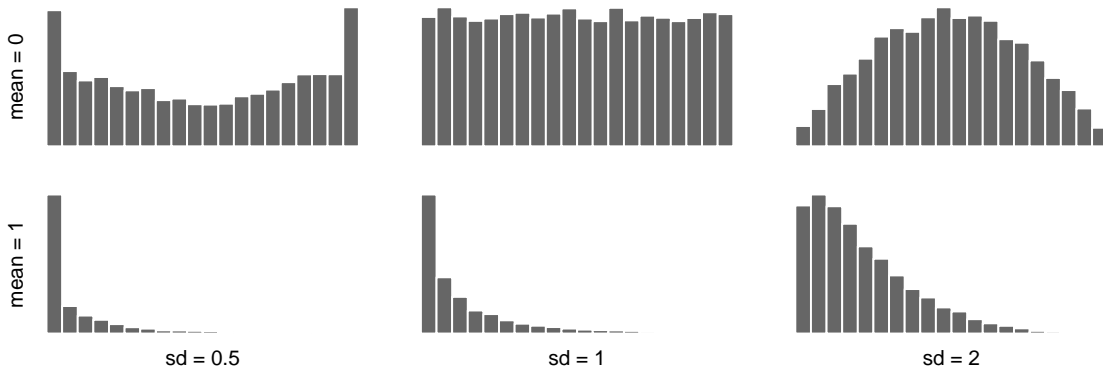


Figure 3: Average rank histograms for observations in $d = 3$ dimensions that follow independent standard Gaussian distributions while the 19 ensemble members follow independent Gaussian distributions with parameters as indicated. The results are based on 10000 repetitions.

3 Histogram shape and the effect of dimensionality

To demonstrate the shape of the histograms under over- and underdispersion as well as bias, we consider a simple simulation experiment where the observations follow an independent standard Gaussian distribution in each dimension. Figure 2 shows band depth rank histograms under this model in a low dimensional setting with $d = 3$ and $m = 20$. The ensemble forecasts are also assumed to follow independent Gaussian distributions with mean $\mu \in \{0, 1\}$ and standard deviation $\sigma \in \{0.5, 1, 2\}$. When the forecasts are underdispersive or have a constant bias, the observation curve is often among the most outlying curves resulting in too many low ranks. Similarly, if the forecasts are overdispersive, the observation curves are too central on average, resulting in too many high ranks. Figure 3 shows the average rank histograms for the same setting. Here, the interpretation of the average ranks is equivalent to that of the standard univariate rank histogram. The histogram shape clearly indicates overdispersion in the forecast through a \cap -shape, underdispersion through a \cup -shape and bias via a skew, triangular shaped histogram.

Figure 4 and 5 demonstrate the effect of increasing dimensionality on the three multivariate ranking methods discussed in Section 2 under under- and overdispersion, respectively. While we

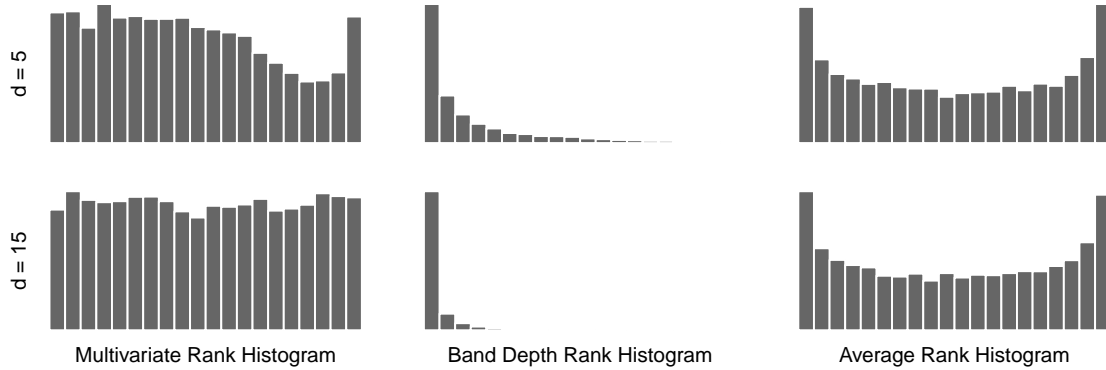


Figure 4: Multivariate ranking of observations in dimension $d = 5$ (top row) and $d = 15$ (bottom row) that follow independent standard Gaussian distributions when the 19 ensemble member forecasts are underdispersed following independent zero-mean Gaussian distributions with standard deviation of 0.5.

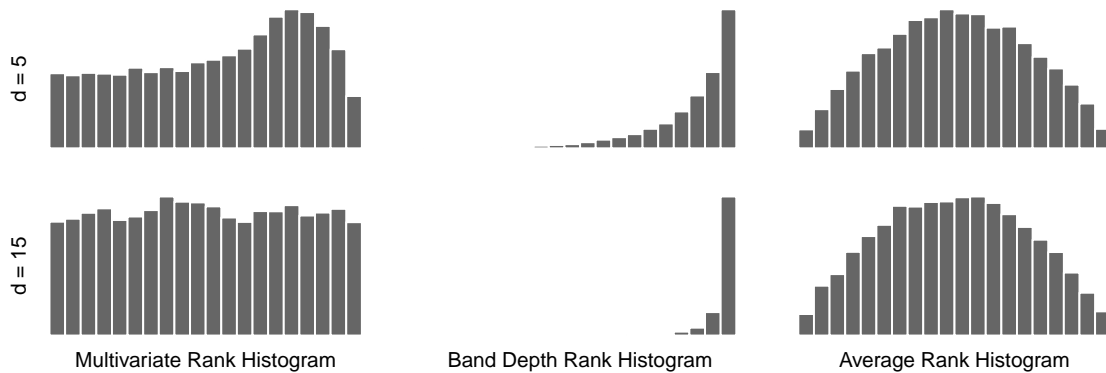


Figure 5: Multivariate ranking of observations in dimension $d = 5$ (top row) and $d = 15$ (bottom row) that follow independent standard Gaussian distributions when the 19 ensemble member forecasts are overdispersed following independent zero-mean Gaussian distributions with standard deviation of 2.

still assume the ensemble consists of 19 members, the dimensionality of the data is here increased to 5 and 15 dimensions. This setting is somewhat unrealistic in that we cannot expect to correctly represent data in 15 dimensions with 29 data points. However, this is often needed in practice as the size of an ensemble forecast is usually limited to a similar magnitude with no additional data available.

The average rank histograms for both examples appear unchanged compared to the low dimensional example in Figure 3 while for the band depth rank, the evidence of miscalibration seem to get stronger with higher dimensions. As reported in Pinson and Girard (2012), we observe identifiability issues with the multivariate ranking of Gneiting et al. (2008) in higher dimensions. In 5 dimensions, only the upper half of the ranks indicates miscalibration and the multivariate rank histograms appear close to uniform when $d = 15$ even though the forecasts are severely miscalibrated. The reason for this can be seen by considering the example in Figure 1, where, due to crossing of the curves, four out of the five curves would obtain a multivariate pre-rank of 1.

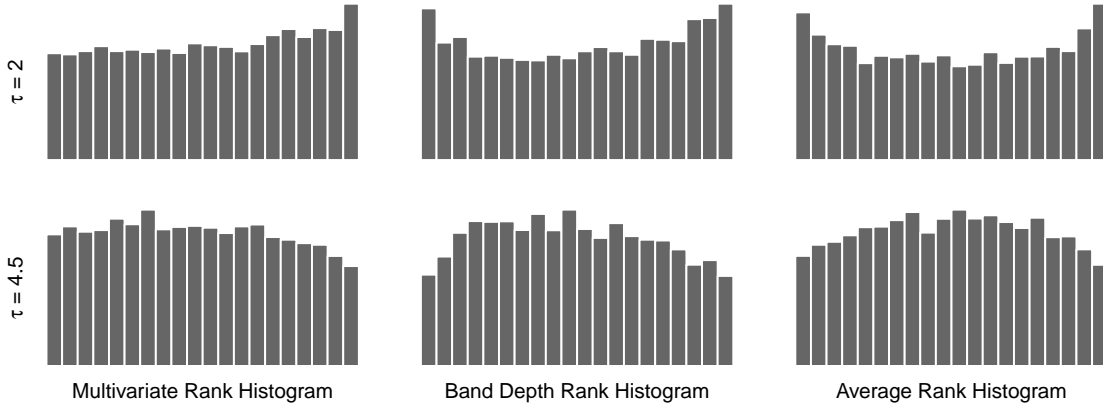


Figure 6: Simulation study to compare the sensitivity of the multivariate rank histogram, the band depth rank histogram and the average rank histogram to misspecification of the dependence structure. The observations follow an AR(1) process at time $t = 1, \dots, 5$ with the dependence structure given in (6) for $\tau = 3$ while the ensemble forecasts follow the same model with $\tau = 2$ (top row) and $\tau = 4.5$ (bottom row). The results are based on 10000 repetitions with 19 ensemble members in each iteration.

4 Assessing deviations in the correlation structure

An appropriate modeling of the correlation between the different components is an important aspect of multivariate predictions. Here, we study the skill of the three multivariate verification methods introduced in Section 2 in detecting misspecification in the correlation structure.

4.1 Gaussian autoregressive processes

Let $\mathbf{y} \in \mathbb{R}^d$ denote a temporal trajectory of a real valued variable observed at d equidistant time points t_1, \dots, t_d . We assume that the observation is a realization of a zero-mean Gaussian AR(1) (autoregressive) process \mathbf{Y} with

$$\text{Cov}(Y_t, Y_{t'}) = \exp(-|t - t'|/\tau), \quad \tau > 0. \quad (6)$$

The process \mathbf{Y} thus has standard Gaussian marginal distributions while the parameter τ controls how fast correlations decay with time lag. We set $\tau = 3$ for \mathbf{Y} and consider ensemble forecasts of the same type but with $\tau = 2$ and $\tau = 4.5$. It follows from this construction that a univariate calibration test at a fixed time point would not detect any miscalibration in the forecasts.

The resulting rank histograms for $d = 5$ and $m = 20$ are shown in Figure 6. While all three calibration assessment methods are able to detect the miscalibration, the multivariate rank histogram suffers from identifiability issues with many low and identical pre-ranks resulting in a flattening out of the left side of the histograms. The band depth and the average rankings, on the other hand, seem quite sensitive to the model misspecification resulting in U-shaped histograms when the correlations decay too fast in the forecasts and \cap -shaped histograms in the opposite situation.

It is not entirely obvious from their definition why the band depth and the average rankings are sensitive to misspecification of the correlation structure. For the latter, this can be demonstrated by comparing the variances of the average rank under different dependence strengths. We first

consider the extreme case where the observations are fully dependent ($\tau = \infty$) and the forecasts are independent ($\tau = 0$) over time. As before, we assume that the different curves are pairwise independent. Due to their independence, the rank of the i th curve is uniformly distributed on $\{1, \dots, m\}$ for each component $k = 1, \dots, d$. Hence, we have

$$\mathbb{E}(\text{rank}_S(x_{ik})) = \frac{m+1}{2}, \quad \text{Var}(\text{rank}_S(x_{ik})) = \frac{m^2-1}{12}, \quad i = 1, \dots, m, \quad k = 1, \dots, d.$$

Assuming the number of forecast curves is high enough, we can neglect the observation curve when calculating the distribution of the average rank of the ensemble curves. Due to the independence of the components of the ensemble members we then get

$$\text{Var}\left(\frac{1}{d} \sum_{k=1}^d \text{rank}_S(x_{ik})\right) \approx \frac{m^2-1}{12d}, \quad i = 1, \dots, m-1.$$

When calculating the average rank of the observation curve, however, we have to take into account that the full dependence over time entails (see appendix)

$$\text{Cov}(\text{rank}_S(x_{mk_1}), \text{rank}_S(x_{mk_2})) = \frac{(m-1)^2}{12}, \quad k_1 \neq k_2.$$

The variance of the average rank of the observation curve is thus

$$\text{Var}\left(\frac{1}{d} \sum_{k=1}^d \text{rank}_S(x_{mk})\right) = \frac{m^2-1}{12d} + \frac{1}{d^2} \left(\sum_{k_1 \neq k_2} \frac{(m-1)^2}{12} \right) = \frac{(m-1)^2}{12} + \frac{m-1}{6d},$$

which is much larger than that of the ensemble members. It is thus more likely that we observe a very low or a very high pre-rank for the observation than for each ensemble member forecast which again leads to proportionally larger number of low and high ranks for the observation resulting in a U-shaped histogram.

Our AR(1) example is less extreme, but the general principle is unaltered. The average rank of the different components concentrates around $\frac{m+1}{2}$ as d increases with stronger serial dependence slowing this convergence. If the serial dependence of the forecasts is too weak, their average ranks concentrate around the mean faster than those of the observations, thus resulting in more extreme observation ranks which cause histograms to be U-shaped. Conversely, if the serial dependence of the forecasts is too strong, their average rank will have a larger variance than the one of the observations, and the average rank histogram will be \cap -shaped. This effect is illustrated in Table 1 for the setup in Figure 6. Indeed, forecasts with too weak serial dependence entail a variance of pre-ranks and ranks that is smaller than that of the observations, while the opposite is true for forecasts with too strong serial dependence.

The effect of misspecified correlation strength on the band depth rank histograms is more complicated since the calculation of ρ_S^{bd} involves squares of $\text{rank}_S(x_{ik})$, and its variance therefore depends on moments of $\text{rank}_S(x_{ik})$ up to order four. The results in Figure 6 and Table 1 indicate that a misspecified correlation structure has a similar effect on the variance of the band depth ranks as applies to the average ranks. The misspecification furthermore has a minor effect on the mean rank of the observation curve as passing from pre-ranks to ranks is a nonlinear transformation and differences in the variance of the pre-ranks may also cause differences of the mean rank. Indeed, the mean value is slightly lower than $\frac{m+1}{2}$ if the forecast correlation is too high and slightly higher otherwise.

Table 1: Mean and variance of simulated pre-ranks and ranks for average ranking and band depth ranking under a zero-mean Gaussian AR(1) model in 5 dimensions with the exponential covariance function in (6). The forecast is a randomly selected ensemble member from an ensemble of size 19. The values are based on 30000 repetitions.

	Average		Band depth	
	Pre-rank	Rank	Pre-rank	Rank
Mean value				
Observation, $\tau = 3$	10.5	10.5	76.0	10.7
Forecast, $\tau = 2$	10.5	10.5	76.0	10.5
Observation, $\tau = 3$	10.5	10.5	76.0	10.2
Forecast, $\tau = 4.5$	10.5	10.5	76.0	10.5
Variance				
Observation, $\tau = 3$	20.0	37.3	332.6	36.8
Forecast, $\tau = 2$	16.5	32.7	277.7	33.3
Observation, $\tau = 3$	19.9	30.0	347.7	29.5
Forecast, $\tau = 4.5$	23.3	33.3	423.0	33.5

4.2 Moving average vs. autoregression

The dependence structure in the preceding example is rather simple with a single parameter τ determining the strength of serial correlations. As a second example, we simulate a forecast ensemble from an AR(1) process with the exponential covariance structure of (6) as before while the observations follow a zero-mean Gaussian MA(4) (moving average) process on t_1, \dots, t_d with identical coefficients such that

$$\text{Cov}(X_{t_i}, X_{t_j}) = \left(1 - \frac{1}{5}|t_i - t_j|\right)_+, \quad (7)$$

where $(\cdot)_+$ denotes the positive part of the term in brackets. That is, the misspecification in the correlation is such that short-term correlations are underestimated while the long-term correlations are overestimated.

Figure 7 shows the resulting histograms for $d = 15$ and $m = 20$. Here, the band depth rank histogram and the average rank histogram complement each other both in their shape and sensitivity. For the example in the upper row of Figure 7, the band depth rank histogram shows a clear divergence from uniformity while both the multivariate rank histogram and the average rank histogram appear close to uniform. In the second example, however, the average rank histogram implies the strongest evidence of miscalibration. This example underscores that the caveats associated with (univariate) rank histograms (Hamill, 2001) also apply here, and different forecasts can lead to histograms with very similar appearance. However, this is a general problem when visualizing a complex object in a single plot, and the above example shows that considering different verification plots of the same object can help safeguard against hasty conclusions on calibration.

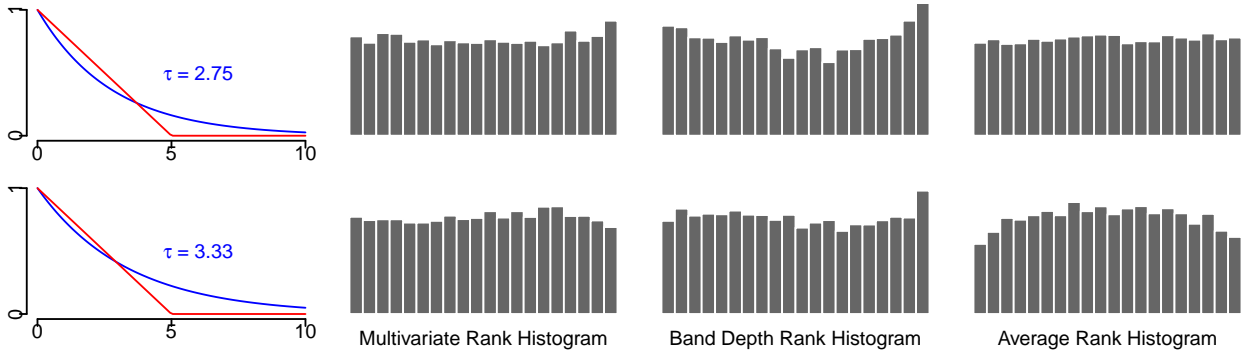


Figure 7: Simulation study to compare the sensitivity of the three multivariate ranking methods to miscalibration in the dependence structure. The observations follow an MA(4) process at time $t = 1, \dots, 15$ with the dependence structure given in (7) (red line) while the forecasts follow an AR(1) process with the covariance function in (6) (blue line), where the scale parameter is $\tau = 2.75$ (top row) and $\tau = 3.33$ (bottom row). The results are based on 10000 repetitions with an ensemble of size 19.

5 Calibration of temperature forecast trajectories

We illustrate the use of the multivariate verification tools discussed above in the setting of probabilistic weather forecasting, where ensembles of weather predictions for the same location, time and weather variable are generated in order to represent forecast uncertainty (Palmer, 2002; Gneiting and Raftery, 2005; Schefzik et al., 2013). Specifically, we consider ensemble temperature forecasts at Berlin Tegel issued by the ensemble prediction system (EPS) of the European center for medium-range weather forecasts (ECMWF) with lead times of 6h, 12h, ..., 72h (Molteni et al., 1996; Leutbecher and Palmer, 2008). The EPS is initialized at 0000 UTC, consists of 50 ensemble members, and will be evaluated during the period from October 10, 2010 to December 31, 2012 using observational data from the local meteorological station as the truth.

The univariate rank histograms (not shown here) suggest that these raw ensemble forecasts have a systematic under forecasting bias at Berlin Tegel and are underdispersive at all considered lead times. We use a simple post-processing method to remove bias and adjust the ensemble spread for each lead time separately. Denoting by \bar{x} the mean of the 50 ensemble members (this is a vector with 12 components, one for each lead time) we obtain a bias-corrected mean μ by fitting a linear regression model $\mu_i = a_i + b_i \bar{x}_i$, separately for each component, to the corresponding observations y_i . For each forecast day the preceding 50 days are taken as training data so that we always have 50 forecast-observation pairs to fit the regression model. This is a compromise between flexible adaptation to seasonal changes on the one hand and gathering sufficient data to permit stable model fitting on the other hand, see e.g. Gneiting et al. (2005) and Raftery et al. (2005).

To adjust the ensemble spread, we use the “error dressing” approach of Roulston and Smith (2003), building a new ensemble by sampling (with replacement) from the forecast errors $\varepsilon_{ij} = y_{ij} - \mu_{ij}$ on the respective training days $j = 1, \dots, 50$ for lead time $i = 1, \dots, 12$. Since the above regression model is fitted to only 50 observation-forecast pairs, there are two potential sources of uncertainty underestimation that need to be taken into account. Firstly, if we were estimating the

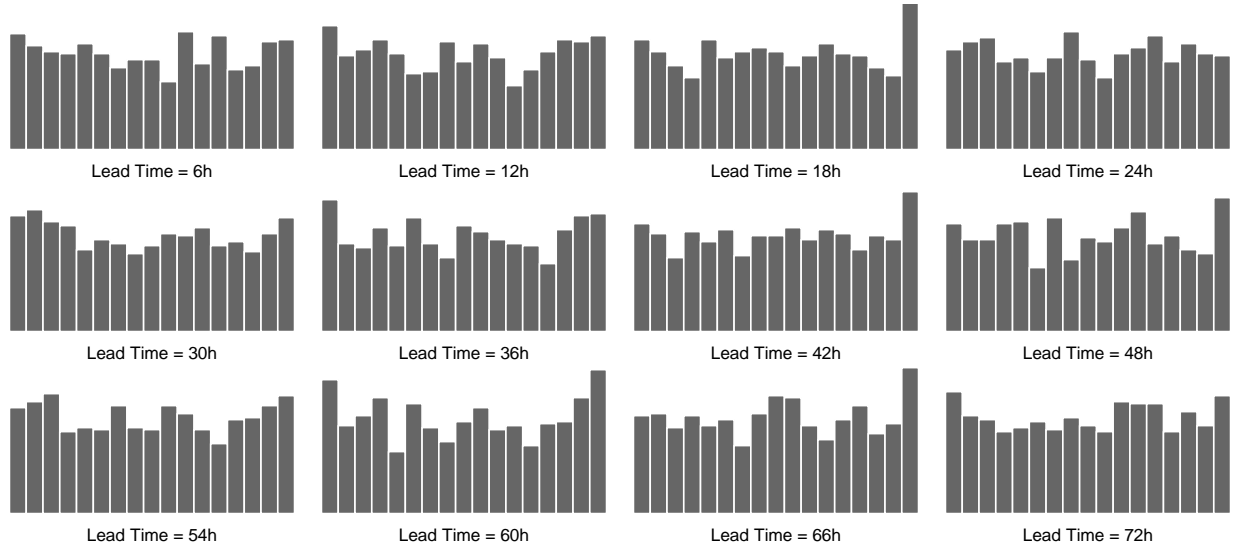


Figure 8: Univariate rank histogram of the bias-corrected error dressing forecasts for lead times 6h, 12h, ..., 72h at Berlin Tegel, each of them based on 823 verification days.

error variance for lead time i , the unbiased estimator would be

$$\hat{\sigma}_i^2 = \frac{1}{48} \sum_{j=1}^{50} \varepsilon_{ij}^2,$$

where the fraction $1/48$ is used instead of $1/50$ to compensate for the fact that a_i and b_i are unknown and must be estimated. To take this into account for error dressing, each ε_{ij} is inflated by a factor $\sqrt{50/48}$. The uncertainty about a_i and b_i also plays a role when prediction intervals are calculated in a regression setting. If we denote by Z_i the design matrix in the above regression problem, \bar{x}_i^* the ensemble mean on the day where a temperature forecast is sought, and $z_i^* = (1, \bar{x}_i^*)'$, the corresponding predictive standard deviation would be $\hat{\sigma}_i \sqrt{1 + z_i^{*'}(Z_i'Z_i)^{-1}z_i^*}$ (Faraway, 2004, Section 3.5). To create an ensemble that represents the corresponding predictive distribution we therefore need to inflate ε_{ij} by the same factor to adjust for the uncertainty of our bias correction. The ensemble obtained in this way is unbiased and nearly calibrated for individual lead times, see Figure 8.

We now consider three different strategies to model dependencies of forecast errors at different lead times,

- (i) ignore multivariate dependencies and perform the error dressing separately for each lead time;
- (ii) perform the error dressing separately for each lead time but use empirical copula coupling (ECC, Schefzik et al., 2013) in a second step to transfer the dependence structure from the raw ECMWF ensemble to the error dressing ensemble;
- (iii) draw the errors from a zero-mean multivariate normal distribution with the empirical covariance matrix of the forecast errors over all lead times, where the variance is inflated as suggested above.

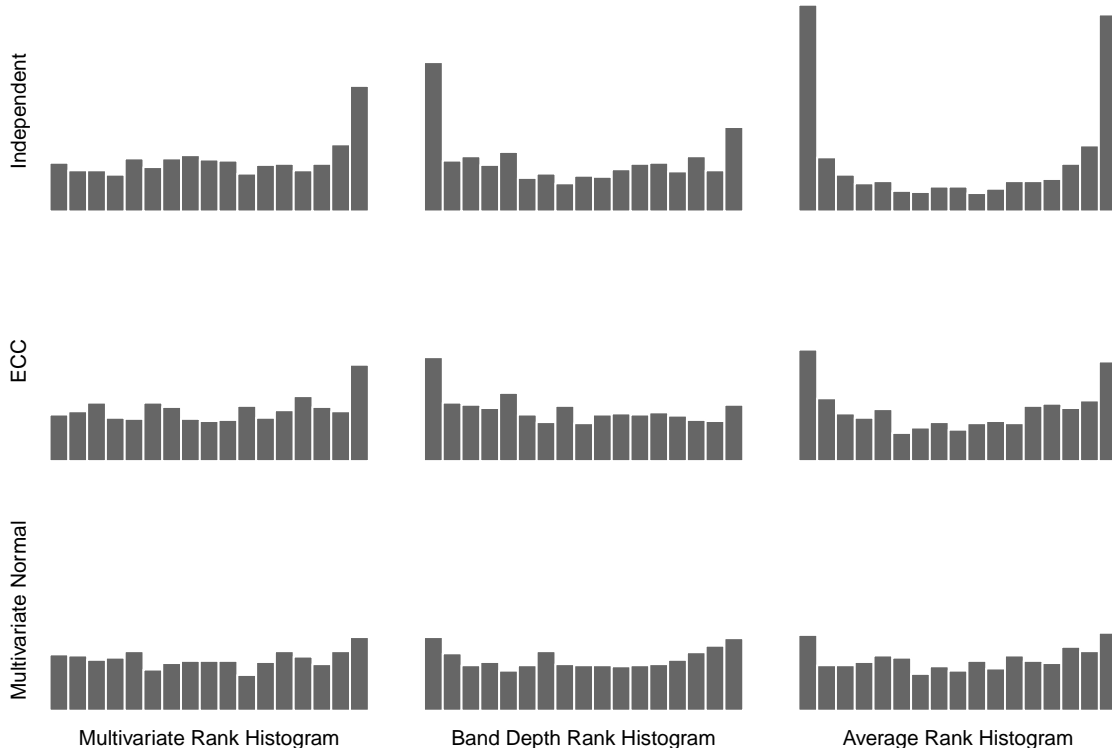


Figure 9: Multivariate rank histograms (left), band depth rank histograms (middle) and average rank histograms (right) of the bias-corrected error dressing forecasts with independent error sampling (top), under ECC (middle) and with multivariate normal error sampling (bottom). The results are based on forecasts for 12 lead times on 823 verification days at Berlin Tegel.

While all three strategies result in similar marginal distributions, the multivariate calibration assessment in Figure 9 reveals substantial differences. When the statistical postprocessing is performed independently for each lead time, both the band depth rank histogram and the average rank histogram exhibit a U-shape indicating a lack of correlation between lead times in the forecasts. Additionally, the band depth rank histogram is skew towards the lowest ranks indicating that the forecasts are too outlying on average. Similar effect is visible in the multivariate rank histogram where the highest ranks are too often assigned to the observation. However, as the average rank histogram is symmetric, we expect the outlying observation curves to have both too low ranks as well as too high ranks on average. Again, we observe here a flattening out of the lower ranks in the multivariate rank histogram due to degeneracy in the pre-ranking; on any given day, at least half the curves are assigned a multivariate pre-rank of 1.

The ECC multivariate postprocessing of Schefzik et al. (2013) significantly improves the calibration of the independent postprocessing, though the observation curves are still somewhat too outlying. For the multivariate normal error sampling, the histograms appear quite close to uniform with a minor divergence towards a U-shape in both the band depth rank histogram and the average rank histogram. An alternative forth multivariate postprocessing option is to apply univariate normal error models followed by ECC. This option leads to calibration results nearly identical to the current results for ECC.

Hamill (2001) pointed out that incorrectly specified covariances between different components

can also be detected by studying the univariate rank histograms of combinations of those components. In the present example of a temporal forecast trajectory, we could e.g. study predicted and observed differences between temperatures at different lead times. If the marginal distributions are calibrated, an ensemble with too strong dependencies between different lead times will underestimate the temperature differences and thus lead to U-shaped rank histograms. Conversely, a lack of dependence will result in \cap -shaped histograms. An analysis of this type confirms the multivariate calibration results of Figure 9: Without multivariate postprocessing, the rank histograms of predicted differences of lags up to 24 hours are strongly \cap -shaped, while the histograms appear close to uniform for both ECC and the multivariate normal postprocessing (results not shown).

6 Discussion

In this paper, we propose two new methods for assessing the calibration of multivariate forecasts where the predictive distribution is represented by a forecast ensemble. Band depth ranking is based on the concept of band depth for functional data, originally proposed by López-Pintado and Romo (2009) and previously employed to create box plots for functional data (Sun and Genton, 2011, 2012; Sun et al., 2013). The somewhat simpler alternative, average ranking, employs the average over the univariate ranks. As demonstrated in several simulated and real data examples, both methods seem to correctly identify various sources of miscalibration in the forecast. Furthermore, they escape the curse of dimensionality affecting the multivariate ranking of Gneiting et al. (2008) as e.g. discussed by Pinson and Girard (2012).

The band depth ranking assesses the centrality of the observation within the forecast ensemble and does not distinguish between positive and negative bias. As a result, the sign of the bias cannot be learned from the shape of the histogram. The method will thus detect miscalibration where the forecasts exhibit a positive bias in a subset of the dimensions and a negative bias in a different subset. In the average ranking, on the other hand, such effects might cancel out. Univariate bias is, however, a miscalibration that can be easily detected through univariate calibration assessment in each dimension. In our opinion, the proposed multivariate techniques should first and foremost complement univariate methods by effectively detecting multivariate features of miscalibration that cannot be found by studying the marginal distributions only.

While calibration is an essential feature of a skillful forecast, a general forecast verification framework should consider a number of different aspects. Gneiting et al. (2007) state that the goal of probabilistic forecasting is to “maximize the sharpness with respect to calibration”. That is, given a group of forecasts that all appear close to calibrated, we should choose the forecast with the highest information content. For predictive distributions or forecast ensembles, this can be attained by choosing the forecast with the smallest spread. More generally, proper scoring rules offer a verification framework under which various aspects of the forecast can be assessed, including calibration and sharpness. A comprehensive review of proper scoring rules is given in Gneiting and Raftery (2007).

Acknowledgments

We thank Marc Genton, Tilmann Gneiting and Alex Lenkoski for sharing their thoughts and expertise. The work of Thordis L. Thorarinsdottir was supported by Statistics for Innovation, *sft*², in Oslo. The work of Michael Scheuerer was supported by the German Federal Ministry of Education and Research, in the framework of the extramural research program of Deutscher Wetterdienst.

Appendix

We assume that we are in the setting of Section 4.1, where both observations and forecasts follow an AR(1) process with correlation structure as given in (6). We derive the expression for the covariance between the ranks $\text{rank}(x_{mk})$ and $\text{rank}(x_{mk'})$ of the k th and k' th component of the observation curve in the entire set of curves, assuming that all curves are independent, that the components of the forecast curves are independent, and that the components of the observation curves are fully dependent (i.e. identical).

Let X_{ik} be the random variable corresponding to the k th component of curve i , f its density and F its cumulative distribution function. The ranks $\text{rank}(X_{mk})$ are then also random quantities and can be written as

$$\text{rank}(X_{mk}) = \sum_{i=1}^m \mathbb{1}\{X_{ik} \leq X_{mk}\}.$$

These quantities are uniformly distributed on $\{1, \dots, m\}$, and hence have mean $\frac{m+1}{2}$ and variance $\frac{m^2-1}{12}$ for every $k \in \{1, \dots, d\}$. Since X_{mk} takes the same value for all k , we further have for $k \neq k'$

$$\begin{aligned} \mathbb{E}(\text{rank}(X_{mk})\text{rank}(X_{mk'})) &= \sum_{i=1}^m \sum_{i'=1}^m P(X_{ik} \leq X_{mk}, X_{i'k'} \leq X_{mk'}) \\ &= 1 + \frac{2(m-1)}{2} + \sum_{i=2}^m \sum_{i'=2}^m P(X_{ik} \leq X_{m\cdot}, X_{i'k'} \leq X_{m\cdot}) \\ &= m + \frac{(m-1)^2}{3} \end{aligned}$$

where we have used that for $i, i' \neq m$ due to independence of the curves

$$P(X_{ik} \leq X_{m\cdot}, X_{i'k'} \leq X_{m\cdot}) = \int_{-\infty}^{\infty} (F(y))^2 f(y) dy = \int_0^1 y^2 dy = \frac{1}{3}.$$

This finally yields

$$\text{Cov}(\text{rank}(X_{mk}), \text{rank}(X_{mk'})) = m + \frac{(m-1)^2}{3} - \frac{(m+1)^2}{4} = \frac{(m-1)^2}{12}, \quad k \neq k'.$$

References

Anderson, J. L. (1996). A method for producing and evaluating probabilistic forecasts from ensemble model integrations. *Journal of Climate* 9, 1518–1530.

- Czado, C., T. Gneiting, and L. Held (2009). Predictive model assesement for count data. *Biometrics* 65, 1254–1261.
- Dawid, A. P. (1984). Statistical theory: The prequential approach (with discussion and rejoinder). *Journal of the Royal Statistical Society Ser. A* 147, 278–292.
- Faraway, J. J. (2004). *Linear Models with R*. Chapman & Hall/CRC.
- Gneiting, T., F. Balabdaoui, and A. E. Raftery (2007). Probabilistic forecasts, calibration and sharpness. *Journal of the Royal Statistical Society Ser. B* 69, 243–268.
- Gneiting, T. and A. E. Raftery (2005). Weather forecasting with ensemble methods. *Science* 310, 248–249.
- Gneiting, T. and A. E. Raftery (2007). Strictly proper scoring rules, prediction, and estimation. *Journal of the American Statistical Association* 102, 359–378.
- Gneiting, T., A. E. Raftery, A. H. Westveld, and T. Goldman (2005). Calibrated probabilistic forecasting using ensemble model output statistics and minimum CRPS estimation. *Monthly Weather Review* 133, 1098–1118.
- Gneiting, T., L. I. Stanberry, E. P. Gritmit, L. Held, and N. A. Johnson (2008). Assessing probabilistic forecasts of multivariate quantities, with applications to ensemble predictions of surface winds (with discussion and rejoinder). *Test* 17, 211–264.
- Hamill, T. M. (2001). Interpretation of rank histograms for verifying ensemble forecasts. *Monthly Weather Review* 129, 550–560.
- Hamill, T. M. and S. J. Colucci (1997). Verification of Eta-RSM short-range ensemble forecasts. *Monthly Weather Review* 125, 1312–1327.
- Leutbecher, M. and T. N. Palmer (2008). Ensemble forecasting. *Journal of Computational Physics* 227, 3515–3539.
- Lichtenstein, S., B. Fischhoff, and L. Phillips (1977). Calibration of probabilities: The state of the art. In H. Jungermann and G. Zeeuw (Eds.), *Decision Making and Change in Human Affairs*, Volume 16 of *Theory and Decision Library*, pp. 275–324. Springer Netherlands.
- Liu, R. (1990). On a notion of data depth based on random simplices. *The Annals of Statistics* 18, 405–414.
- López-Pintado, S. and J. Romo (2009). On the concept of depth for functional data. *Journal of the American Statistical Association* 104, 718–734.
- Möller, A., A. Lenkoski, and T. L. Thorarinsdottir (2013). Multivariate probabilistic forecasting using ensemble Bayesian model averaging and copulas. *Quarterly Journal of the Royal Meteorological Society* 139, 982–991.

- Molteni, R., R. Buizza, T. N. Palmer, and T. Petroliagis (1996). The new ECMWF ensemble prediction system: Methodology and validation. *Quarterly Journal of the Royal Meteorological Society* 122, 73–119.
- Palmer, T. N. (2002). The economic value of ensemble forecasts as a tool for risk assessment: From days to decades. *Quarterly Journal of the Royal Meteorological Society* 128, 747–774.
- Pinson, P. (2013). Wind energy: Forecasting challenges for its operational management. *Statistical Science in press*.
- Pinson, P. and R. Girard (2012). Evaluating the quality of scenarios of short-term wind power generation. *Applied Energy* 96, 12–20.
- Raftery, A. E., T. Gneiting, F. Balabdaoui, and M. Polakowski (2005). Using Bayesian model averaging to calibrate forecast ensembles. *Monthly Weather Review* 133, 1155–1174.
- Roulston, M. S. and L. A. Smith (2003). Combining dynamical and statistical ensembles. *Tellus A* 55, 16–30.
- Schefzik, R., T. L. Thorarinsdottir, and T. Gneiting (2013). Uncertainty quantification in complex simulation models using ensemble copula coupling. *Statistical Science in press*.
- Schuhen, N., T. L. Thorarinsdottir, and T. Gneiting (2012). Ensemble model output statistics for wind vectors. *Monthly Weather Review* 140, 3204–3219.
- Sun, Y. and M. Genton (2012). Adjusted functional boxplots for spatio-temporal data visualization and outlier detection. *Environmetrics* 23, 54–64.
- Sun, Y. and M. G. Genton (2011). Functional boxplots. *Journal of Computational and Graphical Statistics* 20, 313–334.
- Sun, Y., M. G. Genton, and D. W. Nychka (2013). Exact fast computation of band depth for large functional dataset: How quickly can one million curves be ranked? *Stat* 1, 68–74.
- Ziegel, J. F. and T. Gneiting (2013). Copula calibration. arXiv:1307.7650.